Available online at www.sciencedirect.com
ScienceDirect
Journal of the European Ceramic Society 27 (2007) 2433–2444
www.elsevier.com/locate/jeurceramsoc

Chemical corrosion mechanisms of magnesia–chromite and chrome-free refractory bricks by copper metal and anode slag

V. Petkov *, P.T. Jones, E. Boydens, B. Blanpain, P. Wollants

Department of Metallurgy and Materials Engineering, Katholieke Universiteit Leuven, Kasteelpark Arenberg 44, BE-3001 Heverlee, Leuven, Belgium

Received 9 June 2006; received in revised form 14 August 2006; accepted 18 August 2006
Available online 26 September 2006

Abstract

The penetration and corrosion resistance to copper and anode slag of six magnesia–chromite and six chrome-free refractory brick types were tested using static finger tests at a typical copper-refining temperature (1300 °C). The microstructures of the as-delivered and tested refractory types were investigated by means of electron-probe micro-analysis (EPMA) and scanning electron microscopy (SEM) techniques. The results showed that the overall wear rate of the fingers was very low, with the exception of the alumina-based brick made of fused corundum and magnesia–alumina spinel, and the magnesia-based brick made of sintered magnesia and zircon addition. In all refractory types new phases were formed as a result of slag-refractory interactions. Apart from the samples recovered from the copper zone of the latest generation of direct-bonded magnesia–chromite bricks, all the rest were completely infiltrated by copper and slag components (copper oxide, iron oxide, alumina and silica). However, the amount of infiltrated liquid in the chrome-free types was higher than in the magnesia–chromite bricks. Explanations are provided for the distinct infiltration behaviour. The results show that economically viable chrome-free refractory alternatives are still elusive for anode furnace linings.

Keywords: Electron microscopy; Microstructure-final; Refractories; Copper metallurgy

1. Introduction

In copper production magnesia–chromite ("mag-chrome") refractory bricks are typically used to line the smelting, converting and refining furnaces in areas contacting molten matte, metal or slag. Application of other refractory types is largely limited to insulating purposes and the lining of stacks in places where contact with molten phases is unlikely to occur. As a result of the widespread adoption of mag-chrome refractories, nearly all research in the field of copper production furnace linings over the last two decades has focused on this class of material. However, recent environmental initiatives are providing a driving force for the development of new chrome-free refractory types. The specific concern lies in the potential leaching of Cr^{6+} from used mag-chrome bricks. As a result, regulations treating spent mag-chrome bricks as potentially hazardous waste are being enforced, making their disposal difficult and expensive. This has led to the replacement of mag-chrome bricks in other industries; particularly, in cement kilns and steelmaking refining vessels.[1,2] The success of such initiatives may in turn eventually make mag-chrome refractories more difficult to obtain as well as dispose of for copper producers, thus providing further impetus for finding replacement materials.[3] In response to this incentive, Schlesinger et al.[4] aimed at assessing the viability of chrome-free refractory materials, including those containing spinel ($MgAl_2O_4$), as potential replacements for mag-chrome bricks by carrying out static finger tests in copper-containing calcium ferrite slags. The latter are generated in the newer smelting processes, such as the Mitsubishi continuous process. Another set of static,[5] as well as dynamic tests,[6] were performed by the same research team using a fayalite type of slag ($2FeO{\cdot}SiO_2$). As a result of these experiments, it was concluded that none of the tested chrome-free alternatives could match the performance of the mag-chrome reference bricks. Nonetheless, higher-quality magnesia–$MgAl_2O_4$ spinel refractories seemed to have the highest potential as replacement materials. The experiments also highlighted the importance of applying different refractory classes according to the specific melts and conditions characteristic of each furnace type. However, until present no refractory tests appear to have been conducted with the type of slag gen-

* Corresponding author. Tel.: +32 16321318; fax: +32 16321991.
E-mail address: veselin.petkov@mtm.kuleuven.be (V. Petkov).

0955-2219/$ – see front matter © 2006 Elsevier Ltd. All rights reserved.
doi:10.1016/j.jeurceramsoc.2006.08.020

erated during the fire-refining process – the anode slag. This slag differs from the furnace and converter slags by its very high basicity – it typically contains above 50 wt% CuO_x, 30–35 wt% FeO, 7–8 wt% SiO_2 and minor amounts of As, Sb, Pb. With the intention to simulate the melt that exists in a real anode furnace, static finger tests were conducted with magnesia–chromite and chrome-free refractory bricks exposed to copper and anode slag at a typical fire-refining temperature. These corrosion tests are part of a larger research project on the wear mechanisms affecting the bricks in service of industrial anode furnaces with the goal to optimise their refractory lining.[7,8] These lab scale experiments, which should be seen as being complementary to more complex laboratory experiments and industrial studies, focus on refractory corrosion, which is one of the major degradation causes.

2. Experimental

Twelve types of commercially available refractory bricks were tested in the present investigation. Six of them were chrome-free types (A–F) and the other six were mag-chrome based (G–L). Table 1 presents the average bulk compositions and selected properties of the tested refractory products, as indicated by the commercially available data sheets. Four of the chrome-free brick types (A, B, D and E) are based on the magnesia–alumina system, which resembles the magnesia–chrome system in terms of chemistry and phase equilibria. Magnesia–alumina bricks have been successfully used as a replacement for mag-chrome in several applications.[9,10] Types A, B and D are periclase-based refractories with magnesia–alumina (MA) spinel, whereas type E is corundum-based with MA spinel. Two of the chrome-free bricks have a zircon addition (types D and F) while type C has added hercynite spinel. Type B is typically used for lining cement rotary kilns but can also be used in the steel industry.[11,12] Type C was developed specifically for application in the burning section of precalciner kilns.[13] Type D is mostly applied in the furnaces used in cement and lime production, whereas the main application area of type E is the high-wear lining of steel ladles.[14] Finally, type F is specifically produced for application in furnaces for waste incineration and regenerators of glass melting tanks.[14]

The mag-chrome refractory types can be subdivided into two classes: class I – conventional, high-fired (at 1650–1700 °C) direct-bonded bricks, typical of those used in current copper-making furnaces (G–I) and class II – the latest generation of direct-bonded bricks, based on low-in-iron presintered grain and featuring a ceramic bond (J–L).

The experiments were conducted by filling an alumina crucible with 1800 g of electro-refined copper (99.99% Cu) and 500 g of anode slag and then heating it in a laboratory resistance furnace (custom made with SiC heating elements) to 1300 °C. An industrial anode slag with the following composition (in wt%) was used for the experiments: 55 CuO_x, 35 FeO, 8 SiO_2 and minor levels of Pb, Zn, Ni, As and Sb. Four refractory fingers were simultaneously submerged in the molten content of the crucible. Types A–D were tested in the first crucible, types E–H in the second and types I–L in the third one. The dimensions of each finger were 2 cm × 2 cm × 20 cm. The fingers were held in that position for 24 h at a constant temperature of 1300 °C (±5 °C). After completion of the tests, the fingers were withdrawn from the crucible and exposed to ambient air, which resulted in a relatively rapid cooling rate.

It must be noted that some oxidation of the copper phase occurred during the experiments because copper and slag were melted together and because the furnace was not sealed. This was done deliberately to simulate the melt present in an industrial anode furnace, where the oxygen content of copper during fire-refining varies between 0.1 and 1 at% O_2. Therefore, whenever in the text the word "copper" is used, actually "oxidised copper" is meant. This clarification is necessary since it is difficult for pure copper (99.99% Cu) to penetrate the brick microstructure, because of its large wetting angle with periclase (approximately 140° at 1200 °C).[15] However, contaminants (above all, oxygen) can reduce this angle dramatically and thus facilitate infiltration. For example, at a temperature of 1200 °C, the wetting angle between copper and periclase is reduced to less than 90° by an oxygen content of just a few tenths of a percent.[16] The latter

Table 1
Composition and properties of the tested brick types

	Types									
	MgO [wt%]	Cr_2O_3 [wt%]	Al_2O_3 [wt%]	Fe_2O_3 [wt%]	CaO [wt%]	SiO_2 [wt%]	ZrO_2 [wt%]	B.D. [g/cm^3]	A.P. [vol%]	C.C.S. [MPa]
A	93.0	–	2.5	2.5	1.1	0.5	–	3.18	11.5	80
B	87.0	–	10.5	0.5	1.2	0.5	–	2.90	16.0	65
C	91.3	–	3.4	3.8	0.7	0.3	–	3.06	14.0	70
D	94.0	–	2.5	0.2	0.8	0.2	1.4	3.01	14.0	55
E	4.2	–	95.0	0.1	–	0.2	–	3.15	18.5	50
F	78.0	–	–	0.4	0.6	8.0	13.5	3.19	11.0	130
G	60.0	19.0	6.0	13.5	1.3	0.5	–	3.22	17.0	70
H	60.0	19.0	6.0	13.5	1.3	0.5	–	3.22	17.0	70
I	58.0	21.0	6.3	13.0	0.6	0.3	–	3.25	16.5	45
J	62.0	21.5	5.5	9.0	0.8	1.2	–	3.18	16.0	65
K	62.0	23.4	5.0	8.0	0.7	0.9	–	3.31	13.0	105
L*	62.0	23.4	5.0	8.0	0.7	0.9	–	3.31	13.0	105

B.D.: bulk density; A.P.: apparent porosity; C.C.S.: cold crushing strength; (*) kieserite–boric acid impregnated.

creates already wetting conditions and copper penetration is easy and rapid.

3. Sample preparation and analysis technique

Three specimens were cut with a diamond saw from each refractory finger (Fig. 1a). Specimen 1 was recovered from the as-delivered finger, while specimens 2 and 3 were extracted from the tested finger (respectively from the slag and copper zone). Afterwards, the specimens were embedded in a low-viscosity resin (Technovit 4004), ground with diamond plates and polished with diamond suspensions. Finally, carbon was evaporated on sample surfaces to provide a conducting layer for further examination. A JEOL JXA-733 microprobe coupled with an energy dispersive spectroscopy (EDS) system was used for semi-quantitative analysis. The semi-quantitative procedure requires that the operator selects a priori the oxides or elements to be measured. Combinations of elements and oxides (e.g. Fe and MgO) are not possible in the present software configuration. With this electron-probe set up, only elements with atomic numbers ≥Na can be determined. Since oxygen cannot be measured directly, it has to be calculated indirectly from the measured amount of elements and the selected oxide stoichiometry. A high resolution scanning electron microscope (Philips XL-30 FEG), equipped with an EDS detector system with an ultra thin window, was also used for analysing some of the samples and, predominantly, for acquiring high-quality back-scattered electron (BSE) images.

4. Results

Due to their very poor corrosion resistance, two of the fingers were not tested for the full experimental time (24 h) and were, therefore, not considered for detailed disussion in the present paper. The refractory finger type F (magnesia-based brick made of sintered MgO with $ZrSiO_4$ addition) was removed from the crucible after 6 h of testing. This was done to prevent the finger breaking in two, since the area between the copper and slag layer was highly corroded (Fig. 1b). The other refractory type, which proved to be totally inappropriate for the copper/anode slag environment, is type E (alumina-based brick made of fused corundum and magnesia–alumina spinel). About half of this finger was dissolved by the melt after only 4 h of testing (Fig. 1c). This dissolution (together with dissolution of alumina from the crucible wall) somewhat affected the slag composition by increasing its Al_2O_3 content to ∼5 wt%.

4.1. Magnesia–chromite bricks

According to the division of the investigated mag-chrome types made in the experimental part, type H was selected from the first class and type K from the second for a detailed presentation in this paper. These two types are considered representative for their classes and are of considerable interest for the copper industry.

4.1.1. Type H

Fig. 2 presents the microstructure of the as-delivered refractory type H. This is a high-fired direct-bonded mag-chrome brick typical of those used in current copper-making furnaces. This refractory material consists of periclase (almost pure MgO), presintered magnesia–chromite grains, primary and secondary chromite spinel $(Mg,Fe)[Cr,Al,Fe]_2O_4$ and, to a much lesser extent, calcia–magnesia–silicate impurities. The as-delivered microstructure of this refractory type is characterised by a high proportion of direct-bonding between periclase, chromite spinel (primary and secondary) and magnesia–chromite grains, i.e. a direct attachment without any intermediate silicate film.[17] Two types of secondary chromite spinel can be distinguished with

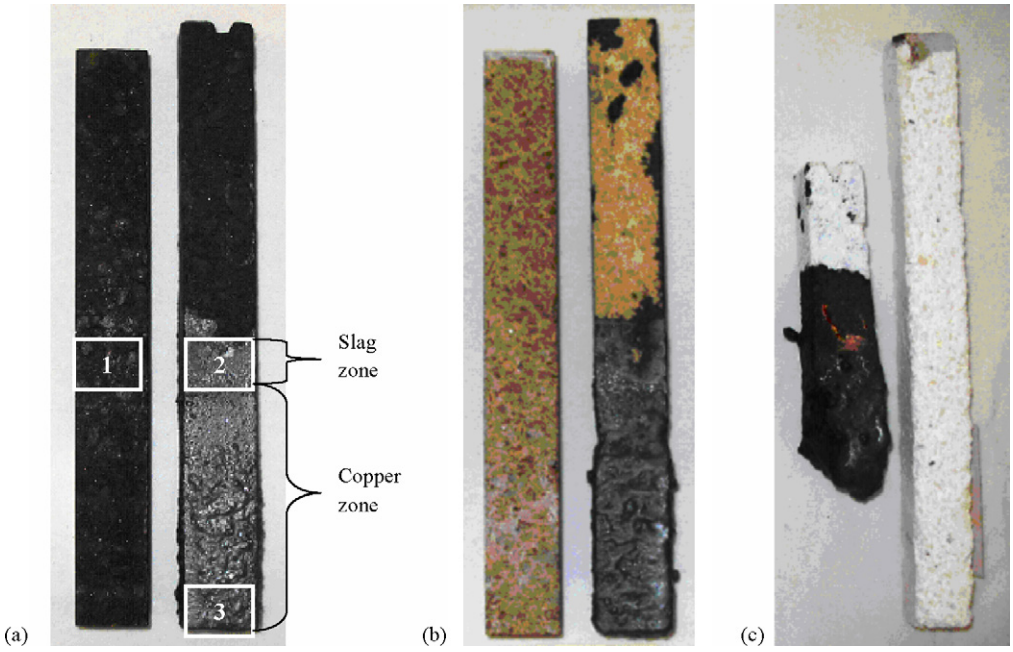

Fig. 1. As-delivered and tested fingers: (a) type K; (b) type F; (c) type E.

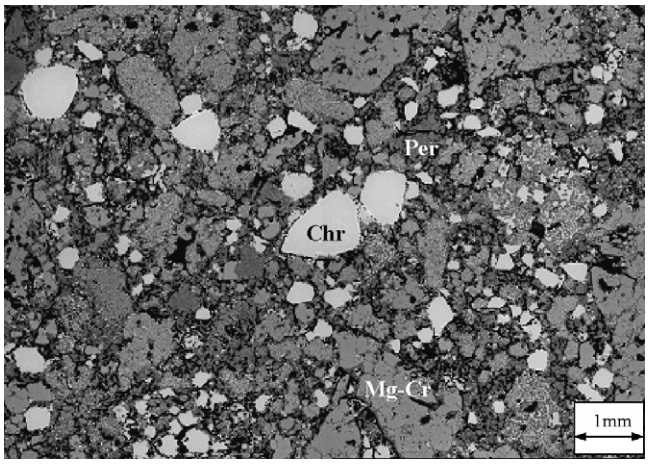

Fig. 2. Overview image of the microstructure of the as-delivered refractory type H. Chr: primary chromite spinel grains, Mg–Cr: presintered magnesia–chromite grains, Per: periclase grains.

respect to their formation mechanism. The first type (intergranular chromite spinel) is formed by intergranular precipitation at the periclase grain boundaries. It can be exsolved out of periclase or crystallised from spinel-rich liquid upon cooling after completion of the firing process. The second type (intragranular chromite spinel) arises from intragranular exsolution precipitation from periclase grains on cooling and thus forms within the grains.[17]

Fig. 3a shows the post-exposure microstructure of refractory H (sample from the slag zone). A layer of frozen melt has formed at the refractory hot face (lower part of the image). It is built up of grey angular grains ('complex spinel') and copper oxide. The complex spinel was formed as a result of reaction between slag (Al_2O_3, FeO, CuO_x) and refractory (MgO, Cr_2O_3) components according to (see Table 2 and phase '1' in Fig. 3b):

$$[MgO]_{refr} + [Cr_2O_3]_{refr} + (Al_2O_3)_{slag} + (FeO)_{slag} + (CuO_x)_{slag} = [(Mg, Cu, Fe^{2+})[Al, Cr, Fe^{3+}]_2O_4]_{refr} \quad (1)$$

where () designates component dissolved in the slag, and [] refers to a solid refractory component. Copper and copper oxide have completely infiltrated the matrix of refractory type H. Microprobe analyses performed on the periclase phase near the hot face ('Per' in Fig. 3b) indicate that a considerable amount of FeO (20 wt%) and CuO_x (5 wt%) diffused into it, as compared to periclase grains in the as-delivered brick, which contain 98–99% MgO. The FeO content of periclase gradually decreases when going deeper into the refractory, analysing 11 wt% in the centre of the sample ('Per' in Fig. 4a), while the amount of CuO_x in periclase remains constant (5 wt%) regardless of the grain location. The centre of a primary chromite grain located at the refractory hot face as well as its rim ('Chr' in Fig. 3b) were analysed revealing that a large amount of FeO diffused in the rim reaching 36 wt% while its quantity in the centre of the grain was only 12 wt%, which corresponds to the average amount of FeO in primary chromite spinel in the as-delivered brick.[8] A similar situation is observed for another slag component – Al_2O_3 – 41 wt% in the rim and 16 wt% in the centre of the

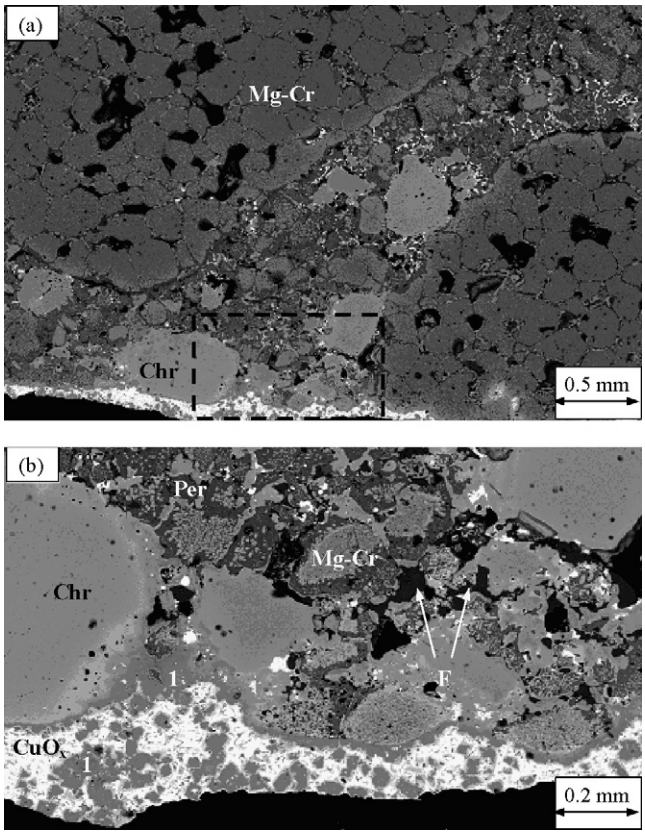

Fig. 3. (a) Overview image of the microstructure of the tested refractory type H (slag zone) and (b) detailed image of the hot face (highlighted area in (a)). Mg–Cr: presintered magnesia–chromite grain, Chr: primary chromite spinel, Per: periclase, F: forsterite, 1: complex spinel phase.

grain. Because of the diffusion of slag components in the rim, the amount of Cr_2O_3 (the major component of primary chromite spinel) has decreased to 3 wt% while in the centre of the grain it analysed 51 wt%. The CuO_x diffusion did not stop at the rim (4 wt%) but reached the centre of the grain (3 wt% CuO_x). The amount of MgO in the hot face primary chromite spinel remains constant (16 wt%) across the whole surface of the grain. The intergranular and the intragranular secondary chromite spinels were analysed in the refractory interior ('Inter' and 'Intra' in Fig. 4a). As expected, the amount of slag components (CuO_x, FeO and Al_2O_3) in the first type of secondary spinel is higher than in the second because infiltration along grain boundaries is much easier than bulk grain diffusion (see Table 2). Another remarkable feature is that a forsterite phase ($2MgO{\cdot}SiO_2$) has formed in the brick as a result of reaction between SiO_2 (slag component) and MgO (refractory component). Analyses performed on this newly-formed phase at the hot face ('F' in Fig. 3b) show that it contains some dissolved FeO (4 wt%). When going deeper in the brick, the amount of penetrated FeO decreases and, therefore, its amount in forsterite also declines (to 2 wt%). The depleting FeO is being replaced by CaO impurities present intergranularly in the refractory microstructure. Analyses performed on the forsterite phase in the centre of the sample (Fig. 4b) show that the latter contains only 1 wt% FeO and already 4 wt% CaO. The SiO_2:MgO ratio in forsterite remains constant in all anal-

Table 2
Compositions of various phases encountered in the tested mag-chrome refractory types

Phases		Mg[a] MgO[b]	Fe[a] FeO[b]	Al[a] Al_2O_3[b]	Cr[a] Cr_2O_3[b]	Ca[a] CaO[b]	Si[a] SiO_2[b]	Cu[a] CuO_x[b]
Type H								
Complex spinel (*hot face*)	Element (at%)	11.1 ± 0.4	13.3 ± 0.4	20.4 ± 0.5	1.3 ± 0.2	–	–	1.6 ± 0.2
	Oxide (wt%)	17.6 ± 0.5	37 ± 1	40 ± 1	2.6 ± 0.2	–	–	4.6 ± 0.2
Copper oxide (*hot face*)	Element (at%)	4.1 ± 0.2	1.4 ± 0.2	3.4 ± 0.2	–	–	1.7 ± 0.2	52 ± 1
	Oxide (wt%)	4.5 ± 0.2	2.7 ± 0.2	4.4 ± 0.2	–	–	2.7 ± 0.2	88 ± 2
Primary chr spinel (*rim*) (*hot face*)	Element (at%)		12.7 ± 0.4	20.7 ± 0.5	2.5 ± 0.2	–	–	2.6 ± 0.2
	Oxide (wt%)	16.7 ± 0.5	36 ± 1	41 ± 1	3.5 ± 0.2	–	–	4.5 ± 0.2
Primary chr spinel (*centre*) (*hot face*)	Element (at%)	10.7 ± 0.4	4.3 ± 0.2	10.7 ± 0.4	18.7 ± 0.5	–	–	1.5 ± 0.2
	Oxide (wt%)	16.9 ± 0.5	12.7 ± 0.4	16.7 ± 0.5	51 ± 1	–	–	30.7 ± 0.2
Intergranular secondary chr (*interior*)	Element (at%)	15.3 ± 0.5	16.7 ± 0.5	12.3 ± 0.4	2.7 ± 0.2	–	–	1.7 ± 0.2
	Oxide (wt%)	22.7 ± 0.5	44 ± 1	22.7 ± 0.5	6.7 ± 0.3	–	–	4.3 ± 0.2
Intragranular secondary chr (*interior*)	Element (at%)	14.2 ± 0.4	10.7 ± 0.4	7.7 ± 0.3	13.7 ± 0.4	–	–	1.3 ± 0.2
	Oxide (wt%)	21.7 ± 0.5	28.7 ± 0.5	13.7 ± 0.4	36 ± 1	–	–	1.7 ± 0.2
Periclase (*hot face*)	Element (at%)	39 ± 1	6.8 ± 0.3	1.3 ± 0.2	1.7 ± 0.2	–	–	2.5 ± 0.2
	Oxide (wt%)	69 ± 2	20.7 ± 0.5	3.7 ± 0.2	3.7 ± 0.2	–	–	5.7 ± 0.2
Periclase (*interior*)	Element (at%)	43 ± 1	3.4 ± 0.2	1.4 ± 0.2	1.7 ± 0.2	–	–	2.5 ± 0.2
	Oxide (wt%)	77 ± 2	11.4 ± 0.4	2.5 ± 0.2	3.4 ± 0.2	–	–	5.5 ± 0.2
CMS (*interior*)	Element (at%)	14.4 ± 0.4	–	–	–	13.5 ± 0.4	15.5 ± 0.4	–
	Oxide (wt%)	27.5 ± 0.5	–	–	–	32 ± 1	40 ± 1	–
Type K								
Complex spinel (*hot face*)	Element (at%)	8.3 ± 0.3	29.3 ± 0.5	9.4 ± 0.3	1.5 ± 0.2	–	–	2.5 ± 0.2
	Oxide (wt%)	10.5 ± 0.4	68 ± 2	15.4 ± 0.5	2.5 ± 0.2	–	–	4.5 ± 0.2
Periclase (*hot face*)	Element (at%)	42 ± 1	5.5 ± 0.3	1.5 ± 0.2	1.1 ± 0.2	–	–	1.3 ± 0.2
	Oxide (wt%)	74 ± 2	15.3 ± 0.5	1.5 ± 0.2	4.3 ± 0.2	–	–	4.3 ± 0.2
Periclase (*interior*)	Element (at%)	44 ± 1	2.5 ± 0.2	1.4 ± 0.2	2.1 ± 0.2	–	–	1.5 ± 0.2
	Oxide (wt%)	82 ± 2	8.3 ± 0.3	1.4 ± 0.2	5.4 ± 0.3	–	–	4.3 ± 0.2
Inter- and intragranular secondary chr (*hot face*)	Element (at%)	14.5 ± 0.4	5.3 ± 0.3	6.4 ± 0.3	18.1 ± 0.5	–	–	–
	Oxide (wt%)	21.4 ± 0.5	14 ± 0.4	12.5 ± 0.4	52 ± 1	–	–	–
CMS (*interior*)	Element (at%)	15.5 ± 0.5	–	–	–	13.1 ± 0.4	15.1 ± 0.5	–
	Oxide (wt%)	28.4 ± 0.5	–	–	–	33 ± 1	39 ± 1	–
Periclase (rim) (*interior*)	Element (at%)	43 ± 1	3.1 ± 0.2	–	–	–	–	–
	Oxide (wt%)	91 ± 2	9.5 ± 0.3	–	–	–	–	–
Grey phase (complex spinel) (*interior*)	Element (at%)	13.3 ± 0.4	8.5 ± 0.3	19.1 ± 0.5	–	–	–	–
	Oxide (wt%)	23.3 ± 0.5	25.1 ± 0.5	50 ± 1	–	–	–	–
Forsterite (*interior*)	Element (at%)	26.1 ± 0.5	–	–	–	–	17.1 ± 0.5	–
	Oxide (wt%)	51 ± 1	–	–	–	–	49 ± 1	–

[a] Element.
[b] Oxide.

ysed locations. The copper oxide phase at the hot face contains a certain amount of dissolved slag and refractory components (see Table 2). Analyses performed deeper in the brick reveal that apart from FeO, the level of impurities in CuO_x gradually diminishes. The copper oxide phase in the centre of the sample contains only 3 wt% FeO and no other species. This seems to suggest that CuO_x and FeO penetrate the brick microstructure concurrently. A calcia–magnesia silicate (CMS) phase (impurity in the raw materials for brick making) was detected in the interior of the sample (Fig. 4b and Table 2).

4.1.2. Type K

Fig. 5a presents the microstructure of the as-delivered refractory type K. The refractory microstructure is very uniform with an even pore distribution throughout the whole sample. Primary chromite grains are few and small in size (0.5–1 mm). Large (up

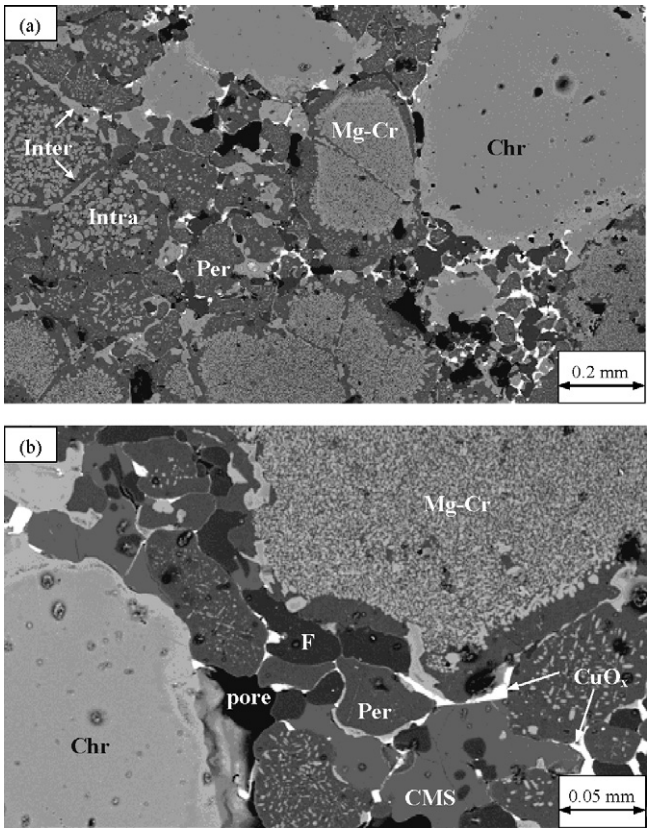

Fig. 4. (a) Detailed image of the microstructure of the tested refractory type H (deeper in the brick-slag zone) and (b) high magnification image of the interior of the tested refractory type H (slag zone). Mg–Cr: presintered magnesia–chromite grain, Chr: primary chromite spinel, Per: periclase, F: forsterite, CMS: calcia–magnesia silicate, Inter: intergranular secondary chromite spinel, Intra: intragranular secondary chromite spinel.

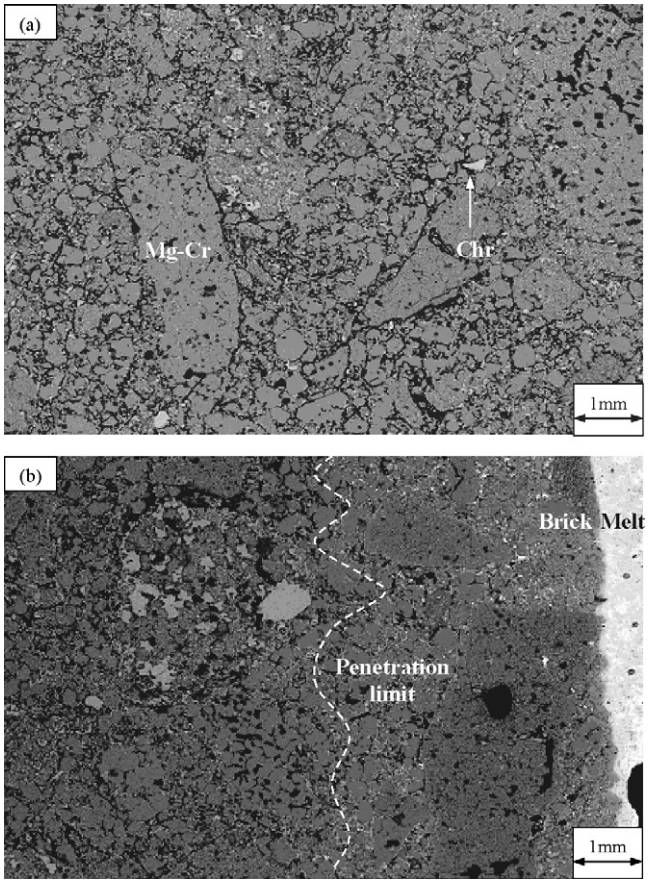

Fig. 5. (a) Overview image of the microstructure of as-delivered refractory type K and (b) overview image of the microstructure of the tested refractory type K (copper zone). Chr: primary chromite spinel, Mg–Cr: presintered magnesia–chromite grain ('oxicrom' sinter).

to 5–6 mm) presintered magnesia–chromite grains with homogeneous dispersion of secondary chromite can be observed.

The bottom part (copper zone) of the refractory finger was not completely infiltrated: the tiny (0.01–0.1 mm) white dots on the image (Fig. 5b) are infiltrated copper. The limit of copper penetration is indicated with a dashed line and is located at a distance of approximately 3–4 mm from the refractory hot face. The penetration resistance of the other two brick types belonging to this class (J and L) was also as high.

The sample recovered from the slag zone was, however, completely infiltrated by CuO_x – small (0.01–0.1 mm) white dots on the image (Fig. 6a). As in the previous mag-chrome sample (type H) a layer of melt has formed at the hot face. The grey angular crystals, better visible in the detailed image ('1' in Fig. 6b), are built up of the same components as the ones found in the complex spinel phase of sample H, only their ratio is different (see Table 2). Forsterite ($2MgO{\cdot}SiO_2$) has also formed in the brick. Analysis performed at the refractory hot face on the newly-formed forsterite phase shows that (like in type H) it contains some dissolved FeO (3 wt%). Microprobe analyses performed on periclase grains near the hot face indicate that a significant amount of FeO (15 wt%) and CuO_x (4 wt%) have diffused into the grains. Similar to the type H sample, the FeO content gradually drops when going deeper into the refractory, analysing 8 wt% in the centre of the sample, while the amount of CuO_x in periclase remains practically constant (4 wt%) regardless of the grain location. Analyses carried out at the hot face show that the amount of infiltrated CuO_x in intergranular and intragranular secondary chromite phases is negligible (below 1 wt%). The compositions of the two types of secondary chromite are practically the same (see Table 2).

4.2. Chrome-free bricks

4.2.1. Type A

Fig. 7a presents an overview of the microstructure of the pre-exposed refractory type A. This is a burnt magnesia–spinel brick made from fused magnesia (MgO) and spinel with a complex composition $(Mg,Fe)[Al,Fe]_2O_4$. Magnesia is present as grains with varying dimensions (0.5–7 mm) as well as finely ground particles (<0.5 mm). A detailed look at the large (>3–4 mm) periclase grains shows that they are comprised of smaller (0.5–1 mm) 'subgrains' with calcia–silicate ($CaSiO_3$) impurities located along their grain boundaries. Discrete spinel grains (Table 3) with varying dimensions (typically between 0.5 and 1 mm) are scattered around the matrix of the brick. An overview of the post-exposure microstructure of refractory A is presented in Fig. 7b. Copper and slag products have completely infiltrated the peri-

Table 3
Compositions of various phases encountered in the tested chrome-free refractory types

Phases		Mg[a] MgO[b]	Fe[a] FeO[b]	Al[a] Al_2O_3[b]	Cr[a] Cr_2O_3[b]	Ca[a] CaO[b]	Si[a] SiO_2[b]	Cu[a] CuO_x[b]
Type A								
Spinel phase (*as-delivered*)	Element (at%)	12.2 ± 0.4	8.1 ± 0.3	21.3 ± 0.5	–	–	–	–
	Oxide (wt%)	24.8 ± 0.5	28.7 ± 0.5	47 ± 1	–	–	–	–
Spinel phase (rim) (*interior*)	Element (at%)	9.2 ± 0.3	28.1 ± 0.5	8.8 ± 0.3	–	–	–	4.1 ± 0.2
	Oxide (wt%)	12.2 ± 0.4	65 ± 2	13.5 ± 0.4	–	–	–	9.2 ± 0.3
Spinel phase (centre) (*interior*)	Element (at%)	9.2 ± 0.3	21.3 ± 0.5	14.1 ± 0.4	–	–	–	1.1 ± 0.2
	Oxide (wt%)	12.8 ± 0.4	56 ± 1	27.1 ± 0.5	–	–	–	4.1 ± 0.2
Complex spinel (*hot face*)	Element (at%)	11.9 ± 0.4	14.1 ± 0.4	15.6 ± 0.5	–	–	–	–
	Oxide (wt%)	20.7 ± 0.5	44 ± 1	35 ± 1	–	–	–	–
Periclase (*interior*)	Element (at%)	48 ± 1	1.1 ± 0.2	–	–	–	–	1.2 ± 0.2
	Oxide (wt%)	92 ± 2	4.2 ± 0.2	–	–	–	–	4.6 ± 0.2
Type B								
Complex spinel (*hot face*)	Element (at%)	11.1 ± 0.4	15.4 ± 0.5	14.1 ± 0.4	–	–	–	–
	Oxide (wt%)	20.6 ± 0.5	45 ± 1	34 ± 1	–	–	–	–
Forsterite (*hot face*)	Element (at%)	26.3 ± 0.5	–	–	–	–	17.9 ± 0.5	–
	Oxide (wt%)	51 ± 1	–	–	–	–	49 ± 1	–
Type C								
Periclase (*interior*)	Element (at%)	42 ± 1	6.1 ± 0.3	1.5 ± 0.2	–	–	–	2.2 ± 0.2
	Oxide (wt%)	74 ± 2	18.7 ± 0.5	3.7 ± 0.2	–	–	–	5.7 ± 0.3
Type D								
Periclase (centre) (*interior*)	Element (at%)	44 ± 1	–	–	–	–	–	–
	Oxide (wt%)	100 ± 2	–	–	–	–	–	–
Periclase (rim) (*interior*)	Element (at%)	43 ± 1	3.7 ± 0.2	–	–	–	–	–
	Oxide (wt%)	91 ± 2	9.5 ± 0.3	–	–	–	–	–
Grey phase (complex spinel) (*interior*)	Element (at%)	13.1 ± 0.4	8.7 ± 0.3	19.7 ± 0.5	–	–	–	–
	Oxide (wt%)	23.3 ± 0.5	25.6 ± 0.5	50 ± 1	–	–	–	–
Forsterite (*interior*)	Element (at%)	26.4 ± 0.5	–	–	–	–	17.2 ± 0.5	–
	Oxide (wt%)	51 ± 1	–	–	–	–	49 ± 1	–

[a] Element.
[b] Oxide.

clase matrix as well as the spinel grains (Fig. 8a). The infiltrated slag imports copper oxide, iron oxide, silica and alumina. The latter comes from external sources – dissolved from the crucible wall and from the high-alumina finger. FeO and CuO_x diffused into the spinel grains, thus changing their composition (Table 3). FeO and Al_2O_3 reacted with MgO following reaction (2), as a result of which a complex spinel phase was formed at the hot face (see '1' in Fig. 8b and Table 3):

$$[MgO]_{refr} + (Al_2O_3)_{slag} + (FeO)_{slag} = [(Mg, Fe^{2+})[Al]_2O_4]_{refr} \quad (2)$$

Up to 3 wt% of CuO_x dissolved in this newly formed phase (see Table 3). The infiltrated silica reacts with magnesia following reaction (3) to form forsterite ('F' in Fig. 8b):

$$(SiO_2)_{slag} + 2[MgO]_{refr} = 2[MgO \cdot SiO_2]_{refr} \quad (3)$$

Up to 4 wt% of FeO can dissolve in the hot face forsterite, while in forsterite formed in the interior of the finger FeO is replaced by CaO (up to 3 wt% CaO). In this way the calcia silicate impurities present in the refractory are incorporated in forsterite formation.

Apart from some small cracks that were infiltrated (Fig. 7b), the large magnesia grains have withstood the attack of the liquid phases. Nevertheless, periclase (even in the interior of the finger) contains around 4 wt% of both diffused iron oxide and copper oxide (Table 3).

4.2.2. Type B

Fig. 9a shows the microstructure of the unexposed refractory type B, which is a burnt magnesia–spinel brick made from sintered magnesia (MgO) and prefabricated spinel ($MgAl_2O_4$). Magnesia is in the form of large grains (but smaller than in type A) and finely ground phase (matrix), while the spinel phase (lighter in colour – BSE mode) is present as grains with varying size (0.5–3 mm).

In Fig. 9b an overview of the microstructure of the exposed finger (copper zone) is presented. Similarly to the previous sample, copper has easily penetrated into the refractory matrix. Some of the spinel grains were also infiltrated (Fig. 10a). The large periclase grains, however, were only partially infiltrated due to the presence of non-stoichiometric intragranular calcia–magnesia silicate impurities, with a chemical formula

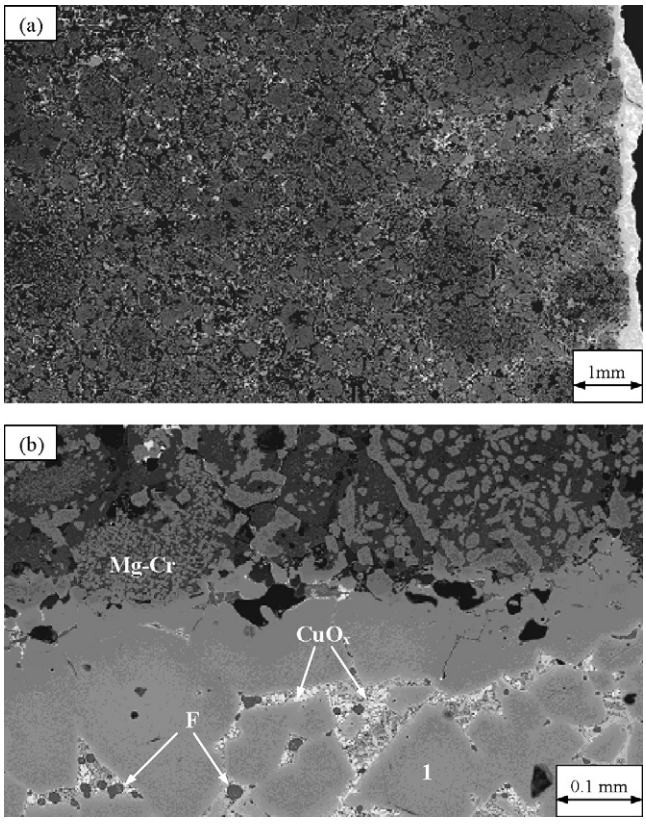

Fig. 6. (a) Overview image of the microstructure of the tested refractory type K (slag zone) and (b) detailed image of the hot face of the tested refractory type K (slag zone). 1: complex spinel phase, F: forsterite, Mg–Cr : 'oxicrom' sinter.

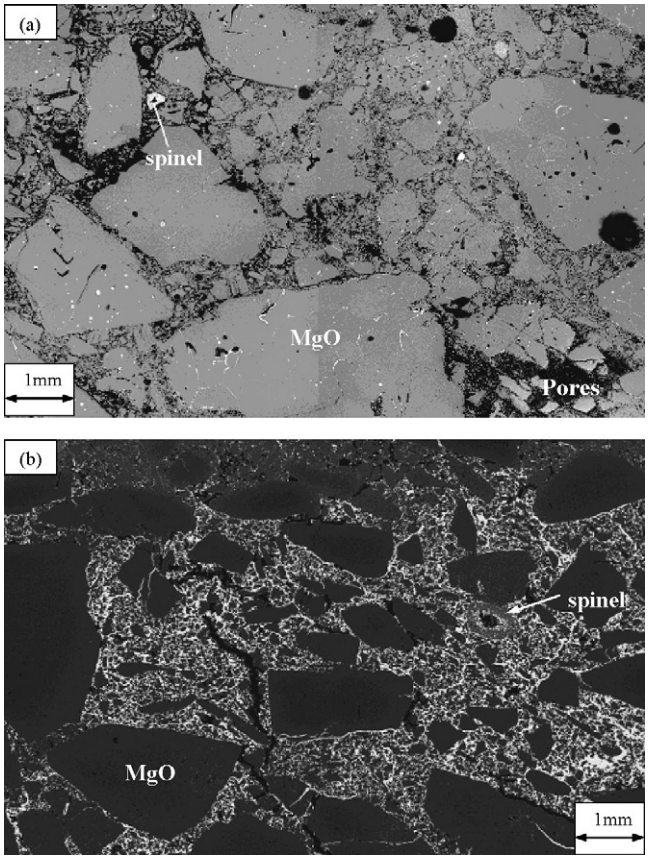

Fig. 7. (a) Overview image of the microstructure of as-delivered refractory type A and (b) overview image of the post-exposure microstructure of refractory type A (slag zone).

closest to $3CaO{\cdot}MgO{\cdot}2SiO_2$. The latter compound has a melting point of 1438 °C,[21] which means that it was entirely solid at the test temperature of 1300 °C and, therefore, acted as a barrier against copper penetration in MgO grains (Fig. 10b). At the hot face of the sample recovered from the slag zone, new phases (complex spinel and forsterite – Fig. 10c, Table 3) were formed as a result of reactions between slag and brick components.

4.2.3. Type C

Fig. 11a illustrates the microstructure of the as-delivered refractory type C. This is a burnt magnesia–spinel brick made of sintered magnesia (MgO) and hercynite spinel ($FeAl_2O_4$). Magnesia is in the form of large grains (up to 7–8 mm) and fine matrix (<0.5 mm) while hercynite is present as grains that vary in size (0.5–5 mm). Fig. 11b shows the result of the exposure to liquid slag of refractory type C. The same reaction (forming $(Mg,Fe)O{\cdot}[Al]_2O_3$) that occurred at the hot face of sample A, has taken place on the surface of the present refractory finger. Forsterite formation has also occurred in this refractory type. Similar to the other brick types, forsterite formed at the hot face contains some FeO (3 wt%), while in forsterite located in the refractory interior FeO was replaced by CaO. The periclase matrix is completely infiltrated by copper oxide (white dots on the image): a global analysis of the sample interior shows more than 6 wt% CuO_x. The liquid phase has easily penetrated into hercynite as well as into magnesia grains. Only a small portion of the magnesia grain boundaries remained protected by the calcia silicate impurities present intragranularly due to the high melting point of $CaO{\cdot}SiO_2$ (1544 °C).[18] However, copper and iron oxides diffused deep in periclase grains. Analyses show virtually the same amount of FeO (18 wt%) and CuO_x (5 wt%) at the rim and inside the grains, which suggests that periclase is prone to diffusion by these two oxides.

4.2.4. Type D

Fig. 12a illustrates the microstructure of the as-delivered refractory type D. This is a burnt special magnesia brick made from sintered magnesia (MgO), spinel ($MgAl_2O_4$) and calcium zirconate ($CaZrO_3$) additive. The $CaZrO_3$ phase (tiny white spots on the image) is evenly distributed throughout the bulk of the sample. The formation of a second bonding phase by addition of fine powder (calcium zirconate – in this case) is supposed to improve the chemical resistance of the brick. Fig. 12b shows the post-exposure microstructure of refractory D (slag zone). The sample was completely infiltrated by copper oxide (white phase on the image). Neither the periclase matrix nor the spinel grains could withstand the attack of the liquid phase. Only the large periclase grains were not thoroughly penetrated. However, analyses show that FeO (up to 9 wt%) diffused in their rim (lighter in colour than the interior). Fig. 12b also shows a common weakness of magnesia-based refractories, namely poor penetration resistance along grain boundaries.[19] The presence of

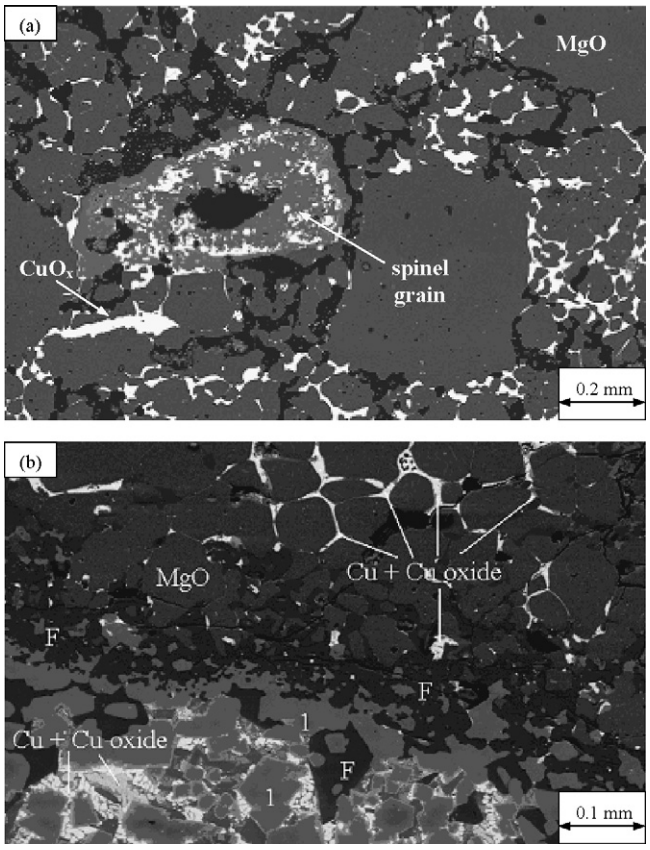

Fig. 8. (a) Detailed image of the post-exposure microstructure of refractory type A (slag zone) and (b) high-magnification image of the slag/refractory interface of the exposed refractory type A (slag zone). 1: Complex spinel phase, F: forsterite.

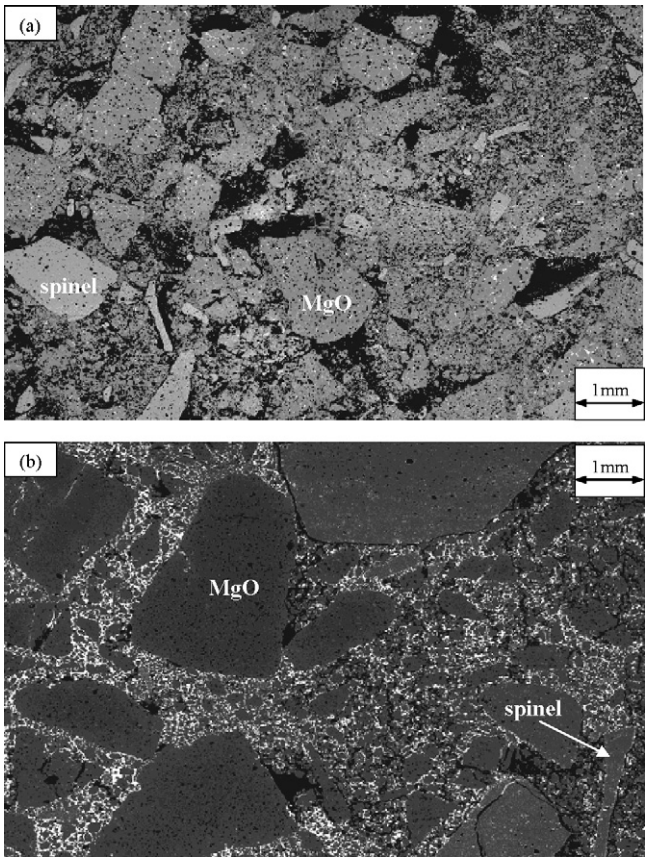

Fig. 9. (a) Overview image of the microstructure of as-delivered refractory type B and (b) overview image of the microstructure of the tested refractory type B (copper zone).

a second bonding phase ($CaZrO_3$) in this brick did not change the above-mentioned pattern, which seems logical since this phase is only present in discrete locations; it does not form a continuous network throughout the refractory microstructure (unlike the secondary chromite spinel in mag-chrome bricks).

5. Wear mechanisms

The overall refractory wear, the depth of infiltration and the level of corrosive reactions for the different refractory classes are summarised in Table 4.

6. Overall wear rate

Having in mind the limited duration (24 h) and the static nature of the finger tests (no motion of the liquid), a low to very low level of refractory wear could be expected. Indeed, the overall wear rate (i.e. the erosion of the refractory surface) was very low, almost zero, with only two exceptions – types E and F. As mentioned earlier, type F – magnesia brick with zirconia content (13.5 wt% ZrO_2) – and especially type E – alumina-based brick (95 wt% Al_2O_3) – were very prone to dissolution in the liquid copper and anode slag. The latter can be explained by the high basicity of the anode slag (55% CuO_x) being in contact with an acidic refractory.

Table 4
Summary of the level of wear, infiltration depth and new phase formation for the tested brick types

Refractory types	Overall wear	Infiltration depth	New phase formation
A: Magnesia-complex spinel $(Mg,Fe)(Al,Fe)_2O_4$	*	***	***
B: Magnesia–MA spinel ($MgAl_2O_4$)	*	***	***
C: Magnesia–hercynite spinel ($FeAl_2O_4$)	*	***	***
D: Magnesia–MA spinel–$CaZrO_3$	*	***	****
E: Alumina–MA spinel	***	***	–
F: Magnesia– $ZrSiO_4$	***	***	–
G–I: Magnesia–chromite, class I	*	**	**
J–L: Magnesia–chromite, class II	*	*	**

(***) High, (**) medium, and (*) low level.

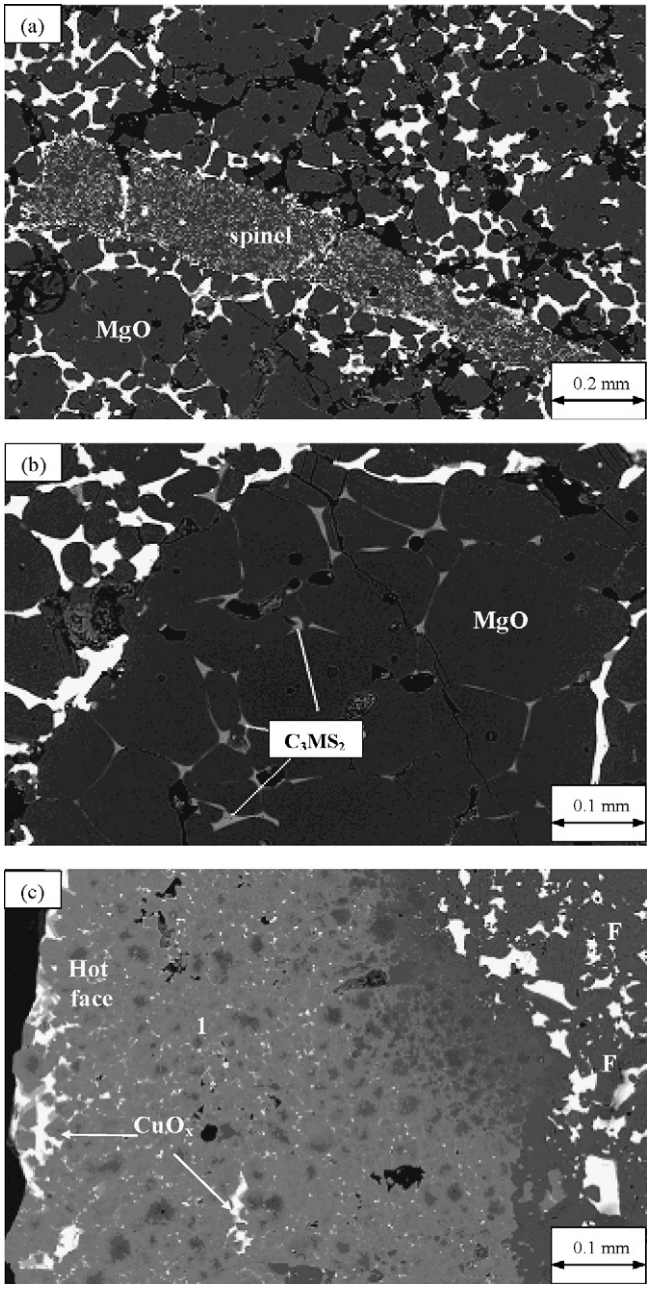

Fig. 10. (a) Spinel grains were easily infiltrated by the copper (refractory type B – copper zone), (b) calcia–magnesia silicate hinders copper infiltration along grain boundaries (refractory type B – copper zone) and (c) detailed image of the hot face of the tested refractory B (slag zone).

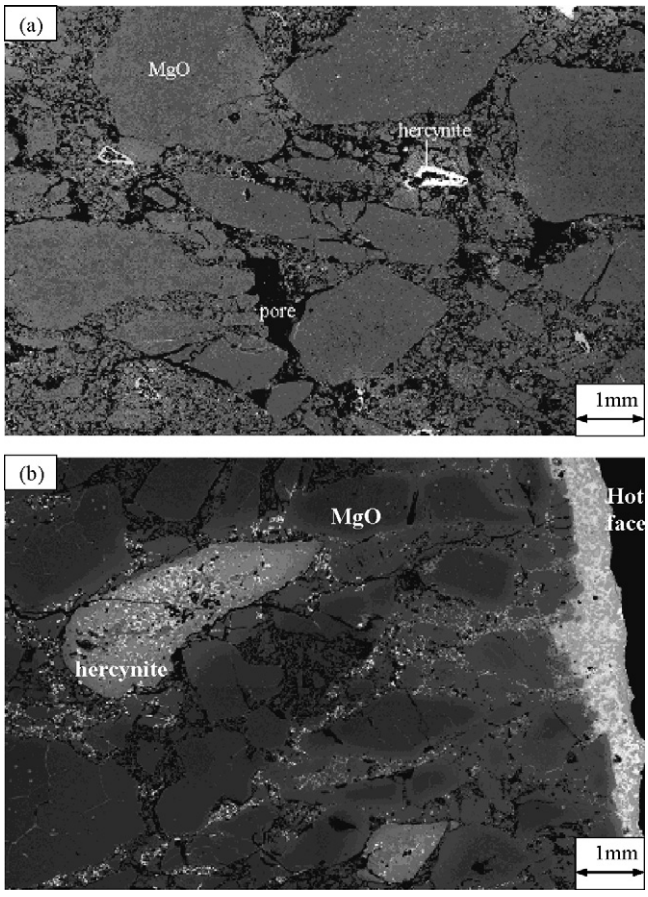

Fig. 11. (a) Overview image of the microstructure of as-delivered refractory type C and (b) overview image of the microstructure of the tested refractory type C (slag zone).

7. Penetration resistance

Apart from the samples recovered from the copper zone of the latest generation of direct-bonded bricks – types J–L – all the rest were completely infiltrated by copper and slag components (copper oxide, iron oxide, alumina and silica). However, the amount of infiltrated liquid in the chrome-free types was higher than the infiltration level in mag-chrome bricks. An explanation for this phenomenon follows.

Considering a single-phase periclase brick being infiltrated along its grain boundaries by a liquid phase, the following state of balance arises when equilibrium is reached:

$$\gamma_{\text{per–per}} = 2\gamma_{\text{per–liq}} \cos\left(\frac{\phi_{\text{per–per}}}{2}\right) \quad (4)$$

where $\gamma_{\text{per–per}}$ is the grain boundary surface energy, $\gamma_{\text{per–liq}}$ the periclase/liquid interfacial energy, and $\Phi_{\text{per–per}}$ is the dihedral angle of the two-phase boundaries formed at the intersection with the grain boundary. $\Phi_{\text{per–per}}$ is thus the angle formed in the neck between neighbouring periclase grains by the liquid phase. The dihedral angle is a measure of the ability of the liquid to penetrate between the grains. No penetration occurs when $\Phi_{\text{per–per}}$ is larger than 120°, whereas low dihedral angles (<60°) result in strong infiltration. Complete penetration occurs when $\Phi_{\text{per–per}}$ is zero. In this case:

$$\gamma_{\text{per–per}} = 2\gamma_{\text{per–liq}} \quad (5)$$

The situation for a refractory brick consisting of two solid phases is more complicated, although similar principles apply. In this case there are three different types of dihedral angles. For a magnesia–chromite brick, which consists of periclase and spinel grains, these are: $\Phi_{\text{per–per}}$, $\Phi_{\text{per–sp}}$ and $\Phi_{\text{sp–sp}}$. Stephenson and White[20] have corroborated that the penetration of a liquid phase between a periclase and a spinel grain is less than between two periclase grains and that this behaviour is due to the interfacial

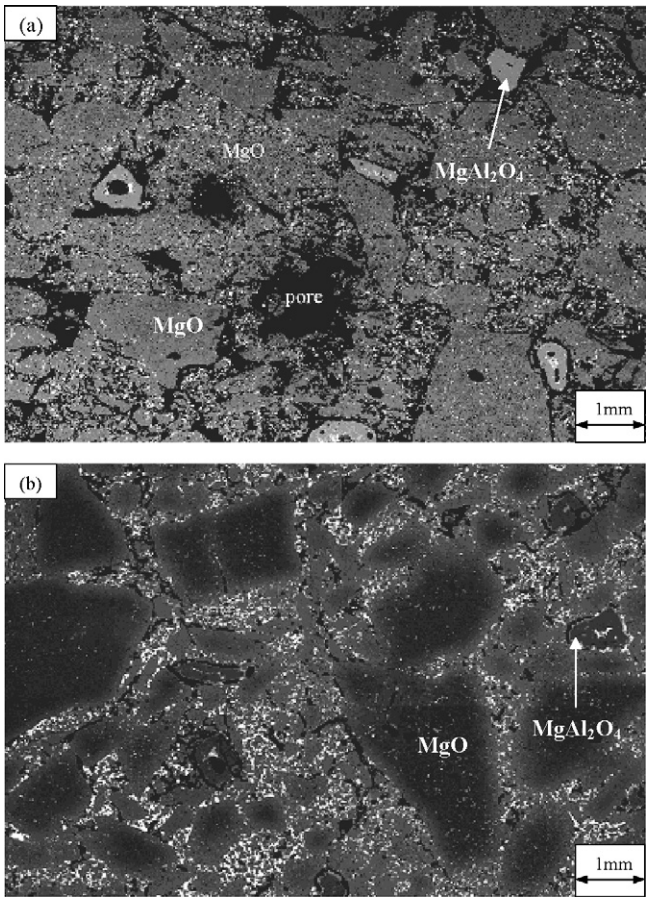

Fig. 12. (a) Overview image of the microstructure of pre-exposed refractory type D and (b) overview image of the microstructure of the tested refractory type D (slag zone).

energy, which is lower between a periclase and a spinel grain than between two periclase grains. This means that the dihedral angle between two periclase grains ($\Phi_{per–per}$) is considerably smaller than the dihedral angle between a periclase and a spinel grain ($\Phi_{per–sp}$).

In the chrome-free bricks tested in this study, the secondary phase (spinel) is present as discrete grains, which do not form a continuous network throughout the refractory microstructure. Besides, the amount of spinel phase is very limited: from ~4 wt% (type D) to ~15 wt% (type B). Therefore, these refractories can be practically considered as single-phase (periclase) bricks, which can be easily infiltrated by Cu/CuO_x as they do not have a meaningful amount of periclase/spinel contacts. On the other hand, in mag-chrome bricks the secondary chromite spinel phase is evenly distributed throughout the refractory microstructure, enveloping magnesia grains (intergranular spinel) and precipitating inside them (intragranular spinel). This particular distribution results in the formation of a continuous spinel network, which renders the dihedral angle between periclase and chromite spinel ($\Phi_{per–sp}$) of primary importance. Furthermore, the amount of spinel (primary and secondary) in the tested mag-chrome refractories is considerable: 44–45 wt%. Since $\Phi_{per–sp}$ is larger than $\Phi_{per–per}$, Cu/CuO_x penetration in mag-chrome bricks is more difficult than in the chrome-free ones and, consequently, the amount of infiltrated liquid in mag-chrome refractories is less. Among all bricks tested, the mag-chrome types J–L showed the highest penetration resistance, i.e. the lowest level of copper and copper oxide infiltration. When discussing the performance of these mag-chrome refractory types, it must be stressed that the samples recovered from the slag zone were thoroughly infiltrated by CuO_x, while the ones recovered from the copper zone were only partially infiltrated by Cu (the centres of the samples were free of infiltration). The explanation of this phenomenon stems from the fact that the wetting angle between copper oxide and periclase is much smaller (about 15° at 1200 °C)[15] than the one between copper and periclase (approximately 140° at 1200 °C)[15] and it is, therefore, much easier for CuO_x to penetrate the brick microstructure.

8. New phase formation

In all refractory types, new phases were formed as a result of slag-refractory interactions. The infiltrating slag brought copper oxide, iron oxide, alumina and silica to the brick. Iron oxide and alumina react with magnesia according to reaction (2). As a result of this interaction a complex spinel phase is formed at the hot face. Its composition is not constant; it varies in the different refractory types (see Tables 2 and 3). Another slag component – silica – reacts with magnesia following reaction (3) to form forsterite. The infiltrated copper does not interact with any refractory components and, therefore, penetrates deeply into the brick. The impact of the formation of these new phases on the refractory performance is difficult to assess. The complex spinel – $(Mg,Fe)[Al]_2O_4$ – was detected only at the hot face while forsterite was analysed throughout the refractory. Although both phases can be found at the refractory hot face, they did not manage to protect the brick from infiltration because the latter preceded their formation.

To assess the impact of forsterite formation throughout the refractory, estimations can be made with respect to the volume expansion/contraction accompanying this formation. Based on the reaction of forsterite formation:

$$2\,\text{moles MgO} + 1\,\text{mole SiO}_2 = 1\,\text{mole Mg}_2\text{SiO}_4, \quad (6)$$

The volume occupied by 2 moles of MgO was calculated (22.4 cm^3) and compared with the volume occupied by the reaction product – 1 mole of Mg_2SiO_4 (43.4 cm^3). The densities of the three compounds are as follows [g/cm^3]: MgO = 3.56–3.68, SiO_2 = 2.26 (tridymite)–2.65 (quartz), Mg_2SiO_4 = 3.22.[21] The comparison shows that a considerable volume expansion (~50%) must occur in the brick when magnesia is transformed into forsterite. On the other hand, considering that this expansion takes place at the border of periclase grains by incorporating liquid silica, one may make an alternative calculation by adding the volume occupied by 1 mole of SiO_2 (23–27 cm^3) to the volume occupied by 2 moles of MgO (22.4 cm^3). The latter sum (45.4–49.4 cm^3) is already very close to the volume occupied by 1 mole of Mg_2SiO_4 (43.4 cm^3) – even some volume shrinkage (5–10%) can be expected. This, together with the filling up of some of the pores by the newly-formed forsterite, explains why bursting or cracking of the fingers was not observed.

9. Conclusions

During the finger tests the chrome-free refractory bricks performed worse than the mag-chrome ones. Two of the former (types E and F) were unable to endure the full duration of the tests while the other four types were easily and thoroughly infiltrated by copper and slag components. The zirconia addition (types D and F) and the two kinds of spinel addition ($MgAl_2O_4$ – in types A and B, $FeAl_2O_4$ – in type C) did not seem to provide any extra benefit to the brick's quality, at least not with regard to Cu and CuO_x penetration resistance. Nevertheless, the above-mentioned additives, known to improve the chemical and thermal shock resistance, respectively, may prove useful in industrial practice, where the bricks are exposed to attack by various species and large temperature fluctuations.[7,8]

It was confirmed that the penetration problem common to periclase-based refractories has not been alleviated by the addition of better bonding materials, such as spinel grain ($MgAl_2O_4$ and $FeAl_2O_4$) and zirconia addition ($ZrSiO_4$ and $CaZrO_3$). The principal reason is that the added phases are not present in the refractory microstructure as a continuous network unlike the secondary chromite phase in mag-chrome bricks. This explains why the penetration resistance of the latter was reasonable. The samples recovered from the copper zone of the latest generation of direct-bonded bricks – types J–L – showed the highest penetration resistance.

There are two main phases present in magnesia–spinel bricks: MgO and $MgAl_2O_4$. During the brick firing process some interdiffusion between these phases occurs. However, the level of interaction is much poorer than the one occuring between MgO and $(Mg,Fe^{2+})[Cr,Al,Fe^{3+}]_2O_4$ (chromite spinel) during firing of mag-chrome bricks. The reason is the low solid solubility of alumina in magnesia (4 wt% Al_2O_3 at 1700 °C) with respect to the solubility of FeO and Cr_2O_3 in magnesia (up to 14 wt% each at 1700 °C).[22] Consequently, during cooling of the bricks no precipitation of a network of intergranular secondary $MgAl_2O_4$ spinel occurs – it remains in discrete positions instead, which results in worse penetration resistance. The only competitive option available nowadays seems to be a technique known as *reinforced spinel bonding*, which involves the introduction of fine, crystalline spinel in the magnesia matrix.[11] Unfortunately, the latter technique will increase the cost of the bricks significantly. Therefore, it can be concluded that an economically viable chrome-free alternative to mag-chrome bricks for application in copper production furnaces remains elusive.

Acknowledgements

The authors of this paper wish to express their appreciation for the financial and operational support of this study provided by Umicore RDI-Olen, Belgium and Cumerio Med-Pirdop, Bulgaria.

References

1. Tsuchinari, A., Okamoto, H. and Yokoyama, Y., Chrome-free refractory for vacuum degassers. In *Proceedings of UNITECR'95, Vol. 2*, 1995, pp. 333–340.
2. Griffin, D. J., Chrome-free generation. *World Cement*, 1996, **27**, 88–92.
3. Crites, M. D., Karakus, M., Schlesinger, M. E., Somerville, M. A. and Sun, S., Interaction of chrome-free refractories with copper smelting and converting slags. *Canadian Metallurgical Quarterly*, 2000, **39**, 129–134.
4. Schlesinger, M. E., Crites, M. D., Sommerville, M. A. and Sun, S., Assessment of spinel-containing refractories for copper smelting and refining. *Journal of the Australian Ceramic Society*, 1998, **34**, 39–44.
5. Schlesinger, M. E., Karakus, M., Crites, M. D., Somerville, M. A. and Sun, S., Chrome-free refractories for copper production furnaces, In *Proceedings of UNITECR '97*, *Vol. 3*, pp. 1703–1709.
6. Crites, M. D. and Schlesinger, M. E., Corrosion testing of chrome-free refractories for copper production furnaces. In *Proceedings of Copper 99 – Cobre 99 International Conference, Vol. 6*, 1999, pp. 187–194.
7. Petkov, V., Jones, P. T., Boydens, E., Blanpain, B. and Wollants, P., A study of industrially worn refractory bricks recovered from a copper anode furnace lining. In *Proceedings of the 47th International Colloquium on Refractories*, 2004, pp. 125–131.
8. Petkov, V., Jones, P. T., Boydens, E., Dekkers, R., Blanpain, B. and Wollants, P., Optimisation of an industrial anode furnace lining using distinct magnesia–chromite refractory qualities. In *Proceedings of UNITECR '05*, 2005, pp. 647–651.
9. Dal Maschio, R., Fabbri, B. and Fiorri, C., Industrial applications of refractories containing magnesium-aluminate spinel. *Industrial Ceramics*, 1988, **8**, 121–126.
10. Wilson, D. R., Evans, R. M., Wadsworth, I. and Cawley, J., Properties and applications of sintered magnesium–aluminium spinels. In *Proceedings of UNITECR '93*, 1993, pp. 749–760.
11. Guo, Z. Q., Palco, S. and Rigaud, M., Reaction characteristics of magnesia–spinel refractories with cement clinker. *International Journal of Applied Ceramic Technology*, 2005, **2**, 327–335.
12. Lampropoulou, P. and Katagas, C., In *Proceedings of the 10th International Congress*, 2004, pp. 97–102.
13. Nievoll, J. and Buchberger, B., *Veitsch-Radex Rundschau*, 1999, **1**, 57–64.
14. Data provided by refractory producer.
15. Barthel, H., Wear of chromium–magnesite bricks in copper smelting furnaces. *Interceramics*, 1981, **30**, 250–258.
16. Tikkanen, M. H., Behaviour of raw copper melts in contact with refractories, *Lecture held on 24/04/1978 in Helsinki, Finland*.
17. Goto, K. and Lee, W. E., The 'direct bond' in magnesia–chromite and magnesia–spinel refractories. *Journal of the American Ceramic Society*, 1995, **78**, 1753–1760.
18. *Slag Atlas, Verein Deutscher Eisenhuttenleute*, Dusseldorf, 1995.
19. Clark, C. B. and Mcdowell, J. S., Basic brick in copper converters—their mineralogical changes. *Journal of Metals*, 1959, **1**, 119–124.
20. Stephenson, I. M. and White, J., Factors controlling microstructure and grain growth in two-phase (one solid + one liquid) and in three phase (two solid + one liquid) systems. *Transactions of the British Ceramic Society*, 1967, **66**, 443–483.
21. Deer, W. A., Howie, R. A. and Zussman, J., *An Introduction to the Rock-Forming Minerals* (*2nd ed.*). Longman Group UK Ltd., 1992.
22. Jones, P. T., Vleugels, J., Volders, I., Blanpain, B., Van der Biest, O. and Wollants, P., A study of slag-infiltrated magnesia–chromite refractories using hybrid microwave heating. *Journal of the European Ceramic Society*, 2002, **22**, 903–916.